Generalized receptor law governs phototaxis in the phytoplankton *Euglena gracilis*

Andrea Giometto[a,b,1], Florian Altermatt[b,c], Amos Maritan[d], Roman Stocker[e], and Andrea Rinaldo[a,f,1]

[a]Laboratory of Ecohydrology, School of Architecture, Civil and Environmental Engineering, École Polytechnique Fédérale de Lausanne, CH-1015 Lausanne, Switzerland; [b]Department of Aquatic Ecology, Eawag: Swiss Federal Institute of Aquatic Science and Technology, CH-8600 Dübendorf, Switzerland; [c]Institute of Evolutionary Biology and Environmental Studies, University of Zurich, CH-8057 Zurich, Switzerland; [d]Dipartimento di Fisica e Astronomia, Università di Padova, I-35131 Padua, Italy; [e]Ralph M. Parsons Laboratory, Department of Civil and Environmental Engineering, Massachusetts Institute of Technology, Cambridge, MA 02139; and [f]Dipartimento di Ingegneria Civile, Edile ed Ambientale, Università di Padova, I-35131 Padua, Italy

Edited by Edward F. DeLong, University of Hawaii, Manoa, Honolulu, HI, and approved April 15, 2015 (received for review December 1, 2014)

Phototaxis, the process through which motile organisms direct their swimming toward or away from light, is implicated in key ecological phenomena (including algal blooms and diel vertical migration) that shape the distribution, diversity, and productivity of phytoplankton and thus energy transfer to higher trophic levels in aquatic ecosystems. Phototaxis also finds important applications in biofuel reactors and microbiopropellers and is argued to serve as a benchmark for the study of biological invasions in heterogeneous environments owing to the ease of generating stochastic light fields. Despite its ecological and technological relevance, an experimentally tested, general theoretical model of phototaxis seems unavailable to date. Here, we present accurate measurements of the behavior of the alga *Euglena gracilis* when exposed to controlled light fields. Analysis of *E. gracilis*' phototactic accumulation dynamics over a broad range of light intensities proves that the classic Keller–Segel mathematical framework for taxis provides an accurate description of both positive and negative phototaxis only when phototactic sensitivity is modeled by a generalized "receptor law," a specific nonlinear response function to light intensity that drives algae toward beneficial light conditions and away from harmful ones. The proposed phototactic model captures the temporal dynamics of both cells' accumulation toward light sources and their dispersion upon light cessation. The model could thus be of use in integrating models of vertical phytoplankton migrations in marine and freshwater ecosystems, and in the design of bioreactors.

phototactic potential | photoresponse | sensory system | photoaccumulation | microbial motility

Microorganisms possess a variety of sensory systems to acquire information about their environment (1), including the availability of resources, the presence of predators, and the local light conditions (2). For any sensory system, the system's response function determines the organism's capability to process the available information and turn it into a behavioral response. Such a response function is shaped by the natural environment and its fluctuations (3–5) and affects the search strategy [be it mate search, food search, etc. (6, 7)] and the swimming behavior of microorganisms (8). Gradient sensing is particularly important in marine and freshwater ecosystems, where the distribution of resources is highly heterogeneous (9, 10) and the ability to move toward resource hot spots can provide a strong selective advantage to motile organisms over nonmotile ones (2, 5). Spatiotemporal patterns of light underwater contribute to the heterogeneity of the aquatic environment. Because light is a major carrier of energy and information in the water column (11), phototaxis is a widespread case of directed gradient-driven locomotion (12, 13), found in many species of phytoplankton and zooplankton. Phototaxis strongly affects the ecology of aquatic ecosystems, contributing to diel vertical migration of phytoplankton, one of the most dramatic migratory phenomena on Earth and the largest in terms of biomass (14). Diel vertical migration is crucial for the survival and proliferation of plankton (13, 15, 16), may affect the structuring of algal blooms (17), and allows plankton to escape from predation by filter-feeding organisms. Because phytoplankton are responsible for one-half of the global photosynthetic activity (18, 19) and are the basis of marine and freshwater food webs (20), their behavior and productivity have strong implications for ocean biogeochemistry, carbon cycling, and trophic dynamics (21, 22).

The quantitative understanding and the associated development of mathematical models for the directed movement of microorganisms have been largely limited to chemotaxis, while other forms of taxis have received considerably less attention despite their ecological importance. For chemotaxis, quantitative experiments have led to a comprehensive characterization of the motile response of bacteria to chemical gradients (23, 24), and this knowledge has been distilled into detailed mathematical models (25). Continuum approaches such as the Keller–Segel model (26, 27), and its generalizations (25), have been used extensively to describe the behavior of chemotactic bacterial populations in laboratory experiments. However, although a limited number of models for phototaxis exists (28–31), an assessment of the phototactic response function is lacking. Existing models rely on untested working hypotheses concerning the cell response to light, originating from the scarcity of experimental work linking controlled light conditions to measured organism responses (*SI Discussion*).

Here, we present quantitative experimental observations of the phototactic response of the flagellate alga *Euglena gracilis* to controlled light gradients. *E. gracilis* is a common freshwater

Significance

Many phytoplankton species sense light and move toward or away from it. Such directed movement, called phototaxis, has major ecological implications because it contributes to the largest biomass migration on Earth, diel vertical migration of organisms responsible for roughly one-half of the global photosynthesis. We experimentally studied phototaxis for the flagellate alga *Euglena gracilis* by tracking algal populations over time in accurately controlled light fields. Observations coupled with formal model comparison lead us to propose a generalized receptor law governing phototaxis of phytoplankton. Such a model accurately reproduces experimental patterns resulting from accumulation and dispersion dynamics. Direct applications concern phytoplankton migrations and vertical distribution, bioreactor optimization, and the experimental study of biological invasions in heterogeneous environments.

Author contributions: A.G., F.A., A.M., R.S., and A.R. designed research; A.G. performed research; A.G., A.M., and A.R. analyzed data; and A.G., F.A., A.M., R.S., and A.R. wrote the paper.

The authors declare no conflict of interest.

This article is a PNAS Direct Submission.

Freely available online through the PNAS open access option.

[1]To whom correspondence may be addressed. Email: andrea.rinaldo@epfl.ch or andrea.giometto@epfl.ch.

This article contains supporting information online at www.pnas.org/lookup/suppl/doi:10.1073/pnas.1422922112/-/DCSupplemental.

phytoplankton species that swims via an anterior flagellum and uses a paraflagellar body and red stigma (a red eyespot) (32) to respond to light gradients. *E. gracilis* has been used extensively as a model organism in both the ecological (33, 34) and the ecophysiological literature (35, 36) and has been used as a candidate species for technological applications such as photobioreactors (37) and micropropellers (38, 39). We use the experimental results to identify a mathematical model for phototaxis. We find that a Keller–Segel-type model (26, 27) accurately describes cell accumulation patterns at all light intensities tested and that the light sensitivity of *E. gracilis* is described by a generalized receptor law (25, 40), a nonlinear function of light intensity that displays a maximum at the light intensity at which cells preferentially accumulate.

Results

We performed laboratory experiments with *E. gracilis* to track the response of algal populations to imposed light conditions. Experiments were conducted in linear channels (5 mm wide × 3 mm high × 2 m long) filled with cells ($2{,}100 \pm 200$ cells·mL^{-1}) suspended in nutrient medium (Fig. 1 and *Materials and Methods*). Light conditions were controlled by light-emitting diodes (LEDs), illuminating the channels from below and operated via Arduino Uno boards (Fig. 1 and *Materials and Methods*). We measured cell distributions in response to localized light sources of different intensity and wavelength λ in the blue ($\lambda = 469$ nm) and red ($\lambda = 627$ nm) regions of the visible spectrum. We measured the light intensity profile $I(x) = I_0\, i(x)$ [we set $i(0) = 1$; Fig. S1; units are retained in I_0] in the linear channels (*Materials and Methods*) and we programmed the LEDs to produce the following peak intensities within the channel, at $x = 0$ cm (above the LED): $I_0 = 0.8$, 2.3, 5.2, 7.8, 10.4, 20.8, 31.3 W·m^{-2} for $\lambda = 469$ nm and $I_0 = 2.6$, 4.7, 10.9, 16.7 W·m^{-2} for $\lambda = 627$ nm. The light profile $i(x)$ was determined by the experimental setting geometry and was invariant for all values of I_0.

Stationary *E. gracilis* accumulation patterns in blue light are shown in Fig. 2 *A*–*G*. Fig. 2 shows that by increasing the peak light intensity I_0 from $I_0 = 0.8$ W·m^{-2} to $I_0 = 5.2$ W·m^{-2}, cell density peaks increase in magnitude (shown are the density profiles normalized by the value at the boundary) and occur in correspondence to the peak in light intensity ($x = 0$ cm). Then, for larger values of I_0, cell density peaks are approximately constant in magnitude, but shift to the left and right of the source. Cell accumulation was maximum at the light intensity $I \simeq I_m = 5.5$ W·m^{-2} (Fig. 2 *A*–*G*; $\lambda = 496$ nm; I_m is calculated using the model proposed in the following paragraphs). Light intensities higher than I_m elicited negative phototaxis (directed movement away from the light source), indicating a biphasic response to light (Fig. 2 *E*–*G*). Such biphasic responses are common in phototaxis, because they allow cells to increase their photosynthetic activity by migrating toward light while preventing damage to the photosynthetic apparatus and cell pigments at excessive light intensities (42, 43). Our experiments showed clearly no response to red light (Fig. 2 *H* and *I*), in line with the reported weak absorption of the *E. gracilis*' eyespot at these wavelengths (44). Red light experiments thus serve as a control that allows us to exclude that the observed cell accumulations toward blue light were due to factors other than phototaxis.

We measured the formation of cell density peaks in time (Fig. 3 *A*–*C*), starting from a homogeneous suspension of cells (Fig. 3*A*), in the presence of a light source of peak intensity $I_0 = 5.2$ W·m^{-2} at $x = 0$ cm. Then, we measured the relaxation of the stationary density peaks after the removal of light (Fig. 3 *D*–*F*). This allowed us to quantify robustly the cell diffusion coefficient, D, due to the random component of the *E. gracilis* motility (45), by fitting the decay rate of the spectral log-amplitudes $\log|\hat{\rho}(k,t)|$ to the square of the wave number (Fig. 3 *G* and *H* and *SI Materials and Methods*). The estimate $D = 0.13 \pm 0.04$ mm^2·s^{-1} is obtained (the SE represents the variability across the first three discrete Fourier transform modes).

The experimental results allowed us to derive a model of phototaxis in *E. gracilis*. We used a Keller–Segel framework, which consists of an advection-diffusion equation for the cell density $\rho(x,t)$ (25) (neglecting cell division owing to the short duration of the experiments):

$$\frac{\partial \rho}{\partial t}(x,t) = \frac{\partial}{\partial x}\left[D\frac{\partial \rho}{\partial x}(x,t) - \frac{d\phi}{dx}[I(x)]\rho(x,t)\right], \qquad [1]$$

where $v_P = d\phi/dx$ is the drift velocity or "phototactic velocity" of the population in the direction of the light gradient. The phototactic velocity was written as the derivative of a phototactic potential, ϕ, which is solely a function of the light intensity $I(x)$ (25). Such reformulation of the Keller–Segel model allows to express the stationary density distribution as a function of $I(x)$. The steady-state accumulation of cells that satisfies Eq. **1**, computed over the spatial extent of the imaging window ($-L \le x \le L$; $L = 6.25$ cm), is as follows:

$$\overline{\rho}(x) = \frac{\rho(x)}{\rho(-L)} = \exp\left[\frac{\phi[I(x)]}{D}\right], \qquad [2]$$

where $\overline{\rho}(x)$ is the normalized cell density appropriate for comparison with experimental observations. Note that, in general, the exponent should be $\phi[I(x)] - \phi[I(-L)]$, but because ϕ is defined only up to an additive constant we set $\phi[I(-L)] = 0$. Thus, ϕ is set to zero for $I = 0$ (Fig. 4*B*).

The stationary cell density distributions under blue light (Fig. 2 *A*–*G*) together with the measured light intensity profiles (Fig. 4*A*) were used to derive the phototactic potential $\phi(I)$ from the data. First, we tested the ability of the Keller–Segel model (Eq. **1**) to capture the observed phototactic responses in different light regimes. Fig. 4*B* (*Inset*) shows that the mean cell density profiles $\overline{\rho}(x)$ collapse on the same curve when plotted together as functions of the light intensity (via Eq. **2**), thus supporting the applicability of Eq. **1** and the computation of ϕ via Eq. **2**, that is, $\phi(I) = D \log \overline{\rho}[x(I)]$. Second, we determined the functional form of the phototactic potential $\phi(I)$. We compared 18 functional forms for $\phi(I)$ using an information-theoretic criterion (46) (*Materials and Methods*). A comparative review of earlier models for phototaxis is provided in *SI Discussion*. The functional forms were chosen by combining monotonically increasing functions of the stimulus I often used to describe sensing, particularly in chemotaxis (25), with monotonically decreasing functions of I,

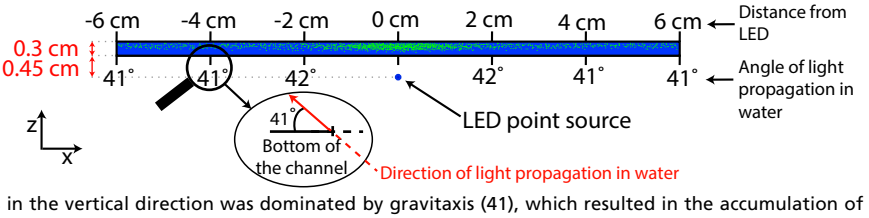

Fig. 1. Sketch of the experimental setup. A LED point source (not to scale) was placed below the linear channels. Individuals of *E. gracilis* (green dots; not to scale) accumulated in the presence of light through phototaxis. Shown are distances from the LED and angles of light propagation in water, computed using Snell's law. The light direction component orthogonal to the channel was disregarded here, because the cells' movement dynamics in the vertical direction was dominated by gravitaxis (41), which resulted in the accumulation of cells at the top of the channel (*SI Materials and Methods* and Fig. S6).

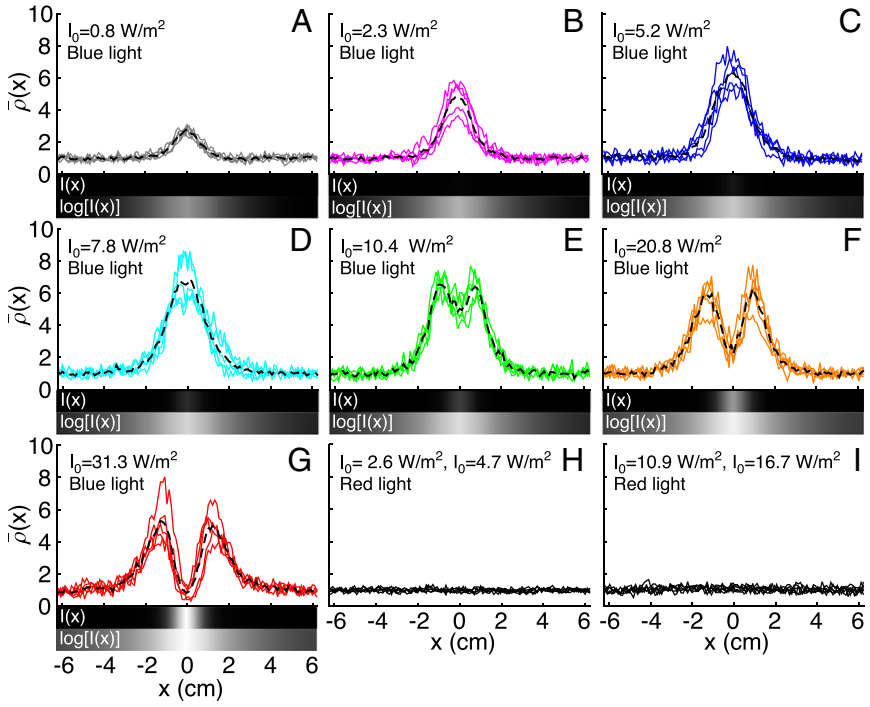

Fig. 2. Phototaxis of *E. gracilis* toward blue and red light of different intensities. Shown are normalized stationary cell density profiles $\bar{\rho}(x)$ around a light source located at $x = 0$ cm for various peak intensities I_0 in the blue (*A–G*; $\lambda = 469$ nm) and red (*H* and *I*; $\lambda = 627$ nm) regions of the visible spectrum. The colored curves in *A–G* are the experimental cell density distributions (five replicates for each value of I_0), and the dashed black lines denote the mean. The gray-scale bars below *A–G* show the imposed blue light intensity profiles $I(x)$, where the gray level scales linearly (upper bar) or logarithmically (lower bar) with I; white corresponds to $I = 31$ W·m^{-2} and black to $I = 0.001$ W·m^{-2}. Positive phototaxis (directed movement toward the light source) is observed with blue light up to $I \simeq I_m = 5.5$ W·m^{-2}, which is the value of light intensity that causes the highest attraction of algae compared with both lower and higher values (*E–G*) of I. For $I > I_m$, negative phototaxis (directed movement away from the light source) is observed. No phototactic behavior is discernible with red light (*H* and *I*) (three replicates for each value of I_0).

accounting for the photophobic behavior shown experimentally at high light intensity.

By fitting each of the above models (Table S1 and Figs. S2 and S3) to the phototactic potential derived from the data (Fig. 4*B*), and by using the Akaike Information Criterion (AIC) (46) to formally quantify their relative performance in simulating the experimental patterns discounting the number of parameters, we conclude that our proposed generalization of the receptor law modified to account for the photophobic behavior shown at high light intensities reads as follows:

$$\phi(I) = aI\frac{I_c - I}{I_r + I}, \qquad [3]$$

where $a = (1.4 \pm 0.04) \cdot 10^{-8}$ m^4·W^{-1}·s^{-1}, $I_r = 1.7 \pm 0.1$ W·m^{-2}, and $I_c = 28.0 \pm 0.3$ W·m^{-2} (SEs are calculated via nonlinear least-squares fitting). The phototactic potential displays a maximum ($\phi = 1.8$ mm^2/s) at $I_m = 5.5$ W·m^{-2} (Fig. 4*B*), the light intensity value that separates the positive and negative phototaxis regimes, and is equal to zero at $I_c = 28.0$ W·m^{-2}. The phototactic velocity $v_P = d\phi/dx$ corresponding to Eq. **3** in our experimental light conditions is shown in Fig. S4. Eq. **3** yields the best model for phototaxis in *E. gracilis* in reproducing the measured stationary cell density profiles (Fig. 4 *C* and *D*).

The proposed phototaxis model, although derived from stationary distributions, correctly captures also the temporal dynamics of phototaxis (red dashed lines in Fig. 3 *A–F*), that is, the formation of density peaks in the presence of light and their subsequent dissipation following light removal (note that Eq. **1** reduces to the diffusion equation in the absence of light stimuli). Small deviations from the model prediction during cell accumulation (Fig. 3 *A–C*) are observed. They are possibly due to the repeated transfers of the channel from the illumination setup to the stereomicroscope for algal density measurements.

Discussion

To compare our experimental setup with natural environments, we note that integrating the ASTM G-173 reference terrestrial solar spectral irradiance (47) in a wavelength window of 10 nm centered at $\lambda = 469$ nm (10 nm is the typical width of emission for our LEDs; *Materials and Methods*) gives a typical irradiance of ~13 W·m^{-2} at sea level. Wavelengths in the blue region of the visible spectrum are among the most transmitted in natural aquatic habitats (11, 48) and penetrate the farthest in the water column, whereas red light is the most attenuated. Thus, the range of light intensities and wavelengths used in the experiments is typical of natural conditions, suggesting that our experimental and theoretical results may have implications for the behavior of phytoplankton in natural environments.

The response of cells to light of different intensities, here expressed in terms of the phototactic potential $\phi(I)$, was inferred from measured stationary cell density profiles. However, the model was shown to capture also the temporal dynamics of cell accumulation around a light source and the diffusive relaxation following light removal. Interestingly, the proposed choice of receptor law, subsumed by $\phi(I)$, includes both positive and negative phototaxis within the same mathematical framework. Although we cannot exclude that phototactic microorganisms may in general sense both the intensity and directionality of light, our model based on intensity alone outperforms other models including both intensity and directionality of light propagation (*SI Discussion*, Fig. S5, and Tables S1–S5), at least for our experimental setting.

Our experimental approach to phototaxis provides a template for the study of ecological processes in shifting and fluctuating resource availability. In fact, the convenient use of programmable LEDs allows one to create microbial microcosms in which light conditions can be accurately controlled to generate a boundless variety of spatiotemporal patterns of environmental stochasticity, affecting both the growth and the movement behavior of cells. Hence, the study system developed here is suggested to be a promising candidate for quantitative microcosm experiments on biological invasions along ecological corridors, range expansions, and source-sink dynamics under environmental noise (49–52).

All things considered, we suggest that the literature lacked an experimentally tested mathematical framework comprising a measure of the phototactic response function of phototactic populations. This work is thus suggested to provide the blueprint for

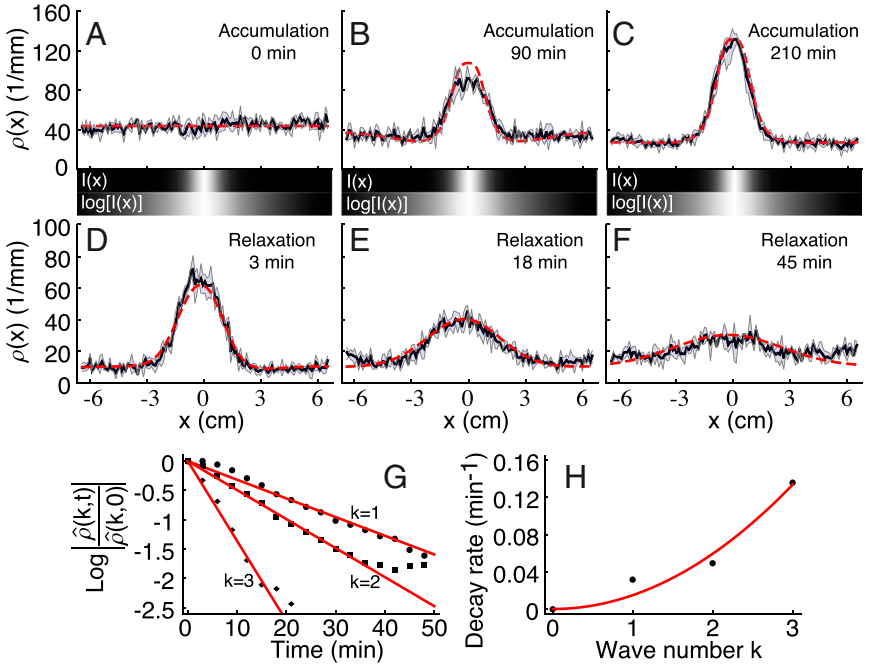

Fig. 3. Temporal dynamics of accumulation around a light source at $x = 0$ cm (*A–C*) and relaxation of cell density peaks upon removal of light (*D–H*). (*A–F*) Experimental cell density profiles at different times. The shaded gray area is delimited by the maximum and minimum cell densities of three replicate experiments and the black line denotes the mean. The red dashed line shows the theoretical prediction, Eq. **1**, using the experimentally determined $\phi(I)$ and $I(x)$ (Fig. 4 *A* and *B*) and D (Table 1) determined experimentally from the relaxation of density peaks (*D–H*). Density profiles are renormalized to display the same mean abundance. The grayscale bars below *A–C* show the light intensity profile imposed during the accumulation; the gray level scales linearly (upper panels) or logarithmically (lower panels) with the intensity I, with white corresponding to $I = 5.2$ W·m^{-2} and black to $I = 0.001$ W·m^{-2}. The temporal decay of Fourier modes (*G*) during the relaxation of density peaks (*D–F*) is exponential [$\log|\hat{\rho}(k,t)/\hat{\rho}(k,t)| = -Dk^2t$; data in black and linear fit in red], and the decay rate is a quadratic function of the wave number k (*H*; data in black and parabolic fit in red), proving the diffusive behavior in the absence of light gradients.

the characterization of the collective response of phytoplankton to light availability and its migration strategies in aquatic ecosystems. Identification of the light intensity regime where positive and negative phototaxis occur pinpoints the regions of the water column where phototactic effects affect the vertical distribution of phytoplankton. Currently, models of phytoplankton growth in contrasting gradients of light and nutrients aimed at reproducing the vertical distribution of phytoplankton, either ignore phototaxis (53) or rely on untested assumptions for the phototactic advection velocity $v_P = d\phi[I(x)]/dx$ (54, 55). The identification of the functional form for $\phi(I)$ provided here can be used directly to integrate realistic predictions for the phytoplankton vertical distribution, which is relevant for global biogeochemical cycles, diversity and coexistence of plankton species, and ecosystem functioning (56, 57). The interspecific variability of the optimal light intensity [defined by $d\phi(I)/dI = 0$] and nutrient requirements have been argued (58) to translate into a sectoring of the water column into separate niches, allowing the coexistence of competitive species.

The mathematical framework derived here may also serve to improve the design of algal bioreactors. Phototaxis of swimming algae, sometimes in combination with other directional behaviors such as gravitaxis (the directed swimming in response to gravity) and gyrotaxis (gravitaxis in the presence of ambient velocity gradients), is speculated to have implications for the design of algal photobioreactors. The phototaxis model proposed here (Eq. **1**) may be used directly to refine existing models for photo-gyrotactic (31) and photo-gyro-gravitactic (59) bioconvection, which currently rely on educated guesses for the phototactic advection term. Our model may be applied to identify optimal designs for cell accumulation far from the reactor surface to avoid biofouling and to achieve enhanced harvesting, a strategy that has been investigated experimentally (37). For example, the fact that the phototactic potential ϕ is much steeper for light intensities above $I_m = 5.5$ W·m^{-2} than below such value, and hence the phototactic velocity is larger for $I > I_m$, suggests that the exploitation of negative phototaxis might be a more effective strategy than the use of positive phototaxis to achieve optimal harvesting.

Algae are also increasingly used in microbiomachine research, for example as micropropellers for the transport of colloidal cargo (38, 39), where light can be used as the external driver of the motion. Although this research is yet to translate into practice, it represents an exciting avenue to harness microbial motility for controlled microscale applications, and phototaxis represents one of the most controllable processes because of the ease of accurately imposing and rapidly modulating external light gradients. The algorithms that are currently used to control such microbiomachines are mostly empirical, and our model may indeed serve to render machine control more robust and accurate. Much attention is currently dedicated to understanding the swimming behavior in these artificial environments (60) and our characterization of collective phototactic dynamics might be exploited to optimize existing technological applications or design new ones.

In the broadest sense, our work provides a blueprint for obtaining robust, quantitative data on directed cell motility, and our method is straightforward to extend to diverse photosynthetic species of plankton, enabling a better understanding of how these important organisms move and live in natural or man-made heterogeneous environments.

Table 1. Parameters describing the phototactic response and movement dynamics of *E. gracilis*

Parameter	Value
Phototactic response	
a	$(1.4 \pm 0.04) \cdot 10^{-8}$ m^4·W^{-1}·s^{-1}
I_r	1.7 ± 0.1 W·m^{-2}
I_c	28.0 ± 0.3 W·m^{-2}
Movement dynamics	
D	0.13 ± 0.04 mm^2·s^{-1}

Values shown are mean ± SE. The parameters a, I_r, and I_c define the phototactic potential ϕ. The diffusion coefficient D was estimated via the relaxation of density peaks (Fig. 3 *D–H*). See *SI Materials and Methods* and Figs. S7 and S8 for measurements of the movement dynamics of individual cells.

Materials and Methods

Algal Culture. The species used in the experiments, *E. gracilis*, was purchased from Carolina Biological Supply and maintained in a nutrient medium (33, 34) composed of sterilized spring water and Protozoan Pellets (Carolina Biological Supply) at a density of 0.45 g·L^{-1}, filtered through a 0.2-μm filter. Algal cultures were initialized 2 wk before the start of the experiment and

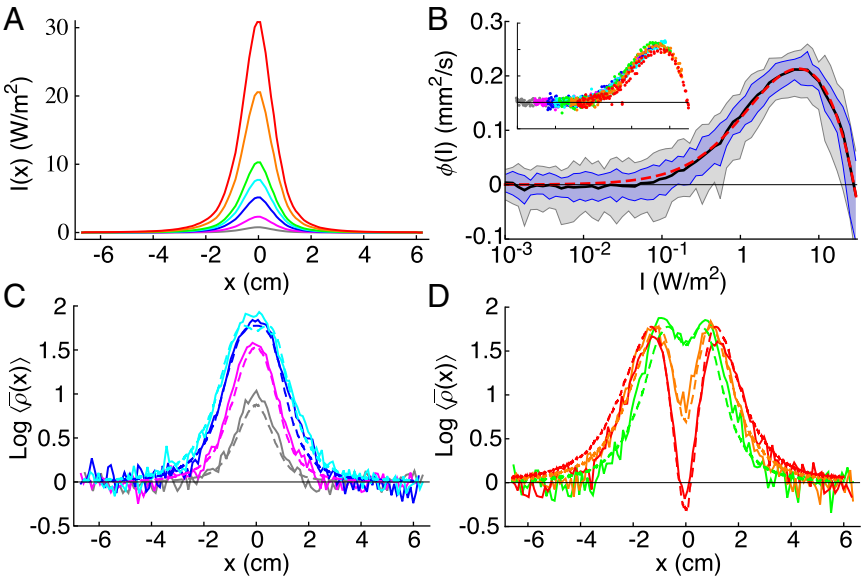

Fig. 4. Computation of the phototactic potential $\phi(I)$. (*A*) Light intensity profiles for different peak intensities I_0. (*B*) Phototactic potential $\phi(I)$ computed from Eq. **2** via inversion of the light intensity profile $I(x)$ (*A*). The solid black line is the mean value of $\phi(I)$ over the stationary density profiles for the various I_0, whereas the blue and gray regions represent the 68% and 95% confidence intervals, respectively. The dashed red line is the best fit of the phototactic potential predicted by the modified receptor law, Eq. **3**. (*Inset*) The phototactic potential calculated from each of the stationary density profiles (color-coded by light intensity regime; see *A* and Fig. 2 *A*–*G*) at different I_0 collapse on the same curve [displayed on the *y* axis is the quantity $\phi(I) = D\log\langle\overline{\rho}(I)\rangle$, where the mean is over the five replicates with same I_0], proving the applicability of Eq. **1**. Axes labels and ticks are as in the enclosing figure. (*C* and *D*) Mean cell density profiles measured at steady state (solid lines) and predicted from Eq. **2** (dashed lines), color-coded according to the light intensity regime (see *A* and Fig. 2 *A*–*G*).

kept at a constant temperature of 22 ° C under constant LED light at $\lambda = 469$ nm. *E. gracilis* individuals have a typical linear size of 14 μm (34), and the duplication time is ∼20 h (33); thus, reproduction can be neglected in our experiments.

Linear Landscapes. The linear landscapes (Fig. 1) used in the experiments were channels drilled on a Plexiglas sheet (61). A second Plexiglas sheet was used as a cover, and a gasket prevented water spillage. Before the introduction of the algal culture to the linear landscapes, the Plexiglas sheets were sterilized with a 70% (vol/vol) ethanol solution, and the gaskets were autoclaved.

Light Sources and Light Intensity Profile. A linear array of LEDs was developed to control the light intensity profile along the linear landscapes. LEDs were placed below the linear channels (Fig. 1). RGB (red, green, blue) LED strips (LED: SMD 5050; chip: WS2801 IC) were controlled via Arduino Uno boards. The LED strips consisted of individually addressable LEDs separated by a distance of 3.12 cm. The light intensity for the B (blue) and R (red) color channels (wavelengths of 463–475 and 619–635 nm, respectively) could be controlled. We measured the total radiant flux emitted by LEDs at the different intensities and wavelengths used with a calibrated photodiode. The relative light intensity profiles, with the LEDs set at the different intensities used, was measured by placing a white paper sheet in the linear channels and measuring the irradiance on the sheet with a digital camera operated in grayscale at fixed aperture, exposure, and distance from the LED. This relative measure of light intensity was converted to absolute values via the total radiant flux measured. In the experiments, periodic light intensity profiles were established with one LED switched on every 12.5 cm. The experimentally measured relative light intensity profile $i(x)$ was found to be well described by the functional form $i(x) = c_0/(x^2 + c_1^2)^2$ (Fig. S1).

Density Measurements. Density profiles were measured at the center of the linear landscape across one entire period of the light intensity profile. Density estimates were obtained by placing the linear landscape under the objective of a stereomicroscope (Olympus SZX16), taking pictures (with the camera Olympus DC72), and counting individuals through image analysis as in ref. 61. Stationary density profiles were measured after 210 min from the introduction of cells in the landscape. In the phototactic accumulation measurements, the landscapes were moved from the support holding the LEDs used for experimentation to the stage of the stereomicroscope just before performing the density measurement. Imaging of the 12-cm imaging window took less than 30 s. Thereby, we assume that no significant relaxation or redistribution of algae occurred during the measurement time. To measure the relaxation of density peaks, the linear landscapes were placed on the stage of the stereomicroscope and the white LED light for microscopy was switched on solely during the measurement time. Landscapes were covered with black cardboard and kept in a dark room to avoid external light during all of the experiments, except during imaging.

Phototactic Potential. To investigate the suitable functional form of the phototactic potential, we combined a set of models that have been used to describe sensing in chemotaxis (25) with a set of monotonically decreasing functions aimed at reproducing the photophobic behavior at high light intensity. The resulting functional forms were formally compared via the AIC to probe their performance in reproducing our laboratory data. The first set, which consists of monotonically increasing functions of light intensity, is as follows: $\phi_1(I) = aI$, $\phi_2(I) = a\,I/(1+bI)$, and $\phi_3(I) = a\log(1+bI)$. These functional forms have been used to describe chemotactic responses (25). The second set consists of monotonically decreasing functions of light intensity I, specifically: $\phi_A(I) = -\log(1+cI)$, $\phi_B(I) = -c\sqrt{I}$, and $\phi_C(I) = -cI$, respectively. The functional forms in the second set were chosen to allow $\lim_{I\to\infty}\phi = -\infty$ (some of the combinations do not satisfy this limiting behavior; e.g., Fig. S3). In fact, experimental observations show that $\overline{\rho}(x) = 0$ if the light intensity in x grows too large. In such case, $\phi(x) = D\log[\overline{\rho}(x)] = -\infty$. Models from the first set were combined with models from the second set both in additive and multiplicative fashions (*SI Materials and Methods*). We fitted all models to the data (Figs. S2 and S3) and computed the corresponding AIC values (Table S1). The best model according to the AIC is $\phi_{2C} = aI(1-cI)/(1+bI)$.

ACKNOWLEDGMENTS. We thank Enrico Bertuzzo, Francesco Carrara, and Lorenzo Mari for discussions and comments, and Antonino Castiglia, Nicolas Grandjean, and Marco Malinverni for support in the light intensity measurement. We gratefully acknowledge the support provided by Swiss Federal Institute of Aquatic Science and Technology (Eawag) discretionary funds; the European Research Council advanced grant program through the project "River Networks as Ecological Corridors for Biodiversity, Populations and Waterborne Disease" (RINEC-227612); and Swiss National Science Foundation Projects 200021_124930/1, 200021_157174, and 31003A_135622. R.S. acknowledges support through a Gordon and Betty Moore Marine Microbial Initiative Investigator Award (GBMF3783).

1. Hazelbauer GL, Berg HC, Matsumura P (1993) Bacterial motility and signal transduction. *Cell* 73(1):15–22.
2. Stocker R (2012) Marine microbes see a sea of gradients. *Science* 338(6107):628–633.
3. Laughlin S (1981) A simple coding procedure enhances a neuron's information capacity. *Z Naturforsch C* 36(9-10):910–912.
4. Kussell E, Leibler S (2005) Phenotypic diversity, population growth, and information in fluctuating environments. *Science* 309(5743):2075–2078.
5. Celani A, Vergassola M (2010) Bacterial strategies for chemotaxis response. *Proc Natl Acad Sci USA* 107(4):1391–1396.
6. Mesibov R, Ordal GW, Adler J (1973) The range of attractant concentrations for bacterial chemotaxis and the threshold and size of response over this range. Weber law and related phenomena. *J Gen Physiol* 62(2):203–223.
7. Shoval O, et al. (2010) Fold-change detection and scalar symmetry of sensory input fields. *Proc Natl Acad Sci USA* 107(36):15995–16000.
8. Lazova MD, Ahmed T, Bellomo D, Stocker R, Shimizu TS (2011) Response rescaling in bacterial chemotaxis. *Proc Natl Acad Sci USA* 108(33):13870–13875.
9. Levin SA (1994) Patchiness in marine and terrestrial systems: From individuals to populations. *Philos Trans R Soc Lond B Biol Sci* 343(1303):99–103.

10. Azam F (1998) Microbial control of oceanic carbon flux: The plot thickens. *Science* 280(5364):694–696.
11. Ragni M, Ribera D'Alcala M (2004) Light as an information carrier underwater. *J Plankton Res* 26(4):433–443.
12. Bhaya D (2004) Light matters: Phototaxis and signal transduction in unicellular cyanobacteria. *Mol Microbiol* 53(3):745–754.
13. Jékely G, et al. (2008) Mechanism of phototaxis in marine zooplankton. *Nature* 456(7220):395–399.
14. Hays GC (2003) A review of the adaptive significance and ecosystem consequences of zooplankton diel vertical migrations. *Hydrobiologia* 503(1-3):163–170.
15. Ringelberg J, Flik BJG (1994) Increased phototaxis in the field leads to enhanced diel vertical migration. *Limnol Oceanogr* 39(8):1855–1864.
16. Kingston MB (1999) Effect of light on vertical migration and photosynthesis of *Euglena proxima* (Euglenophyta). *J Phycol* 35(2):245–253.
17. Smayda TJ (1997) Harmful algal blooms: Their ecophysiology and general relevance to phytoplankton blooms in the sea. *Limnol Oceanogr* 42(5 Pt 2):1137–1153.
18. Field CB, Behrenfeld MJ, Randerson JT, Falkowski P (1998) Primary production of the biosphere: Integrating terrestrial and oceanic components. *Science* 281(5374): 237–240.
19. Behrenfeld MJ, et al. (2006) Climate-driven trends in contemporary ocean productivity. *Nature* 444(7120):752–755.
20. Chassot E, et al. (2010) Global marine primary production constrains fisheries catches. *Ecol Lett* 13(4):495–505.
21. Falkowski PG, Barber RT, Smetacek V (1998) Biogeochemical controls and feedbacks on ocean primary production. *Science* 281(5374):200–207.
22. Boyce DG, Lewis MR, Worm B (2010) Global phytoplankton decline over the past century. *Nature* 466(7306):591–596.
23. Adler J, Hazelbauer GL, Dahl MM (1973) Chemotaxis toward sugars in *Escherichia coli*. *J Bacteriol* 115(3):824–847.
24. Barbara GM, Mitchell JG (2003) Bacterial tracking of motile algae. *FEMS Microbiol Ecol* 44(1):79–87.
25. Tindall MJ, Maini PK, Porter SL, Armitage JP (2008) Overview of mathematical approaches used to model bacterial chemotaxis II: Bacterial populations. *Bull Math Biol* 70(6):1570–1607.
26. Keller EF, Segel LA (1970) Initiation of slime mold aggregation viewed as an instability. *J Theor Biol* 26(3):399–415.
27. Keller EF, Segel LA (1971) Model for chemotaxis. *J Theor Biol* 30(2):225–234.
28. Burkart U, Häder DP (1980) Phototactic attraction in light trap experiments: A mathematical model. *J Math Biol* 10(3):257–269.
29. Torney C, Neufeld Z (2008) Phototactic clustering of swimming microorganisms in a turbulent velocity field. *Phys Rev Lett* 101(7):078105.
30. Vincent RV, Hill NA (1996) Bioconvection in a suspension of phototactic algae. *J Fluid Mech* 327:343–371.
31. Williams CR, Bees MA (2011) Photo-gyrotactic bioconvection. *J Fluid Mech* 678:41–86.
32. Jékely G (2009) Evolution of phototaxis. *Philos Trans R Soc Lond B Biol Sci* 364(1531): 2795–2808.
33. Altermatt F, et al. (2015) Big answers from small worlds: A user's guide for protist microcosms as a model system in ecology and evolution. *Methods Ecol Evol* 6(2): 218–231.
34. Giometto A, Altermatt F, Carrara F, Maritan A, Rinaldo A (2013) Scaling body size fluctuations. *Proc Natl Acad Sci USA* 110(12):4646–4650.
35. Wolken J (1961) *Euglena: An Experimental Organism for Biochemical and Biophysical Studies* (Rutgers Univ Press, New Brunswick, NJ).
36. Vallee BL, Falchuk KH (1993) The biochemical basis of zinc physiology. *Physiol Rev* 73(1):79–118.
37. Ooka H, Ishii T, Hashimoto K, Nakamura R (2014) Light-induced cell aggregation of *Euglena gracilis* towards economically feasible biofuel production. *R Soc Chem Adv* 4(40):20693–20698.
38. Itoh A (2004) *Euglena* motion control by local illumination. *Bio-mechanisms of Swimming and Flying*, eds Kato N, Ayers J, Morikawa H (Springer, Tokyo), pp 13–26.
39. Itoh A, Tamura W (2008) Object manipulation by a formation-controlled *Euglena* group. *Bio-mechanisms of Swimming and Flying*, eds Kato N, Kamimura S (Springer, Tokyo), pp 41–52.
40. Lapidus IR, Schiller R (1976) Model for the chemotactic response of a bacterial population. *Biophys J* 16(7):779–789.
41. Häder DP, Griebenow K (1988) Orientation of the green flagellate, *Euglena gracilis*, in a vertical column of water. *FEMS Microbiol Ecol* 53(3-4):159–167.
42. Häder DP, Lebert M (1998) The photoreceptor for phototaxis in the photosynthetic flagellate *Euglena gracilis*. *Photochem Photobiol* 68(3):260–265.
43. Lebert M, Porst M, Richter P, Hader DP (1999) Physical characterization of gravitaxis in *Euglena gracilis*. *J Plant Physiol* 155(3):338–343.
44. Strother GK, Wolken JJ (1960) Microspectrophotometry of *Euglena* chloroplast and eyespot. *Nature* 188(4750):601–602.
45. Ahmed T, Stocker R (2008) Experimental verification of the behavioral foundation of bacterial transport parameters using microfluidics. *Biophys J* 95(9):4481–4493.
46. Burnham KP, Anderson DR (2002) *Model Selection and Multimodel Inference: A Practical Information-Theoretic Approach* (Springer, New York), 2nd Ed.
47. ASTM International (2008) Standard tables for reference solar spectral irradiances, direct normal and hemispherical on 37° tilted surface. ASTM Standard G173 (ASTM International, West Conshohocken, PA).
48. Jeffrey S (1984) Responses of unicellular marine plants to natural blue-green light environments. *Proceedings in Life Sciences*, ed Senger H (Springer, Berlin), pp 497–508.
49. Gonzalez A, Holt RD (2002) The inflationary effects of environmental fluctuations in source-sink systems. *Proc Natl Acad Sci USA* 99(23):14872–14877.
50. Bertuzzo E, et al. (2007) River networks and ecological corridors: Reactive transport on fractals, migration fronts, hydrochory. *Water Resour Res* 43(4):W04419.
51. Rodriguez-Iturbe I, et al. (2009) River networks as ecological corridors: A complex systems perspective for integrating hydrologic, geomorphologic and ecologic dynamics. *Water Resour Res* 45(1):W01413.
52. Méndez V, Llopis I, Campos D, Horsthemke W (2011) Effect of environmental fluctuations on invasion fronts. *J Theor Biol* 281(1):31–38.
53. Greenwood J, Craig P (2014) A simple numerical model for predicting vertical distribution of phytoplankton on the continental shelf. *Ecol Modell* 273:165–172.
54. Klausmeier CA, Litchman E (2001) Algal games: The vertical distribution of phytoplankton in poorly mixed water columns. *Limnol Oceanogr* 46(8):1998–2007.
55. Mellard JP, Yoshiyama K, Litchman E, Klausmeier CA (2011) The vertical distribution of phytoplankton in stratified water columns. *J Theor Biol* 269(1):16–30.
56. Steele JH, Yentsch CS (1960) The vertical distribution of chlorophyll. *J Mar Biol Assoc UK* 39(2):217–226.
57. Lampert W, McCauley E, Manly BFJ (2003) Trade-offs in the vertical distribution of zooplankton: Ideal free distribution with costs? *Proc Biol Sci* 270(1516):765–773.
58. Yoshiyama K, Mellard JP, Litchman E, Klausmeier CA (2009) Phytoplankton competition for nutrients and light in a stratified water column. *Am Nat* 174(2):190–203.
59. Williams CR, Bees MA (2011) A tale of three taxes: Photo-gyro-gravitactic bioconvection. *J Exp Biol* 214(Pt 14):2398–2408.
60. Garcia X, Rafaï S, Peyla P (2013) Light control of the flow of phototactic microswimmer suspensions. *Phys Rev Lett* 110(13):138106.
61. Giometto A, Rinaldo A, Carrara F, Altermatt F (2014) Emerging predictable features of replicated biological invasion fronts. *Proc Natl Acad Sci USA* 111(1):297–301.